INL/CON-09-16348
PREPRINT

Performance of Single Electrode-Supported Cells Operating in the Electrolysis Mode

IMECE 2009

J. E. O'Brien
G. K. Housley
D. G. Milobar
Nathalie Petigny

November 2009

The INL is a
U.S. Department of Energy
National Laboratory
operated by
Battelle Energy Alliance

Proceedings of the 2009 International Mechanical Engineering Congress and Exposition
IMECE2009
November 13 – 19, 2009, Lake Buena Vista, Florida, USA

IMECE2009 - 11683

PERFORMANCE OF SINGLE ELECTRODE-SUPPORTED CELLS OPERATING IN THE ELECTROLYSIS MODE

J. E. O'Brien, G. K. Housley
Idaho National Laboratory
Nuclear Science and Engineering
Idaho Falls, ID, USA

D. G. Milobar
U. of Arizona,
Dept. of Mechanical Eng.
Tucson, AZ, USA

Nathalie Petigny
Saint-Gobain
High-Performance Materials
Cavaillon, France

ABSTRACT

An experimental study is under way to assess the performance of electrode-supported solid-oxide cells operating in the steam electrolysis mode for hydrogen production over a temperature range of 800 to 900ºC. Results presented in this paper were obtained from single cells, with an active area of 16 cm^2 per cell. The electrolysis cells are electrode-supported, with yttria-stabilized zirconia (YSZ) electrolytes (~10 μm thick), nickel-YSZ steam/hydrogen electrodes (~1400 μm thick), and manganite (LSM) air-side electrodes. The experiments were performed over a range of steam inlet mole fractions (0.1 – 0.6), gas flow rates, and current densities (0 to 0.6 A/cm^2). Steam consumption rates associated with electrolysis were measured directly using inlet and outlet dewpoint instrumentation. On a molar basis, the steam consumption rate is equal to the hydrogen production rate. Cell performance was evaluated by performing DC potential sweeps at 800, 850, and 900°C. The voltage-current characteristics are presented, along with values of area-specific resistance as a function of current density. Long-term cell performance is also assessed to evaluate cell degradation. Details of the custom single-cell test apparatus developed for these experiments are also presented.

INTRODUCTION

There is a growing interest in the development of large-scale non-fossil hydrogen production technologies. This interest is driven by the immediate demand for hydrogen for refining of increasingly low-quality petroleum resources (e.g., the Athabasca oil sands, coal) [1, 2], the expected intermediate-term demand for carbon-neutral synthetic fuels [3], and the possible long-term demand for carbon-free hydrogen as an environmentally benign transportation fuel [4].

High-temperature nuclear reactors have the potential for substantially increasing the efficiency of hydrogen production from water, with no consumption of fossil fuels, no production of greenhouse gases, and no other forms of air pollution. Water-splitting for hydrogen production can be accomplished via high-temperature electrolysis (HTE) or thermochemical processes, using high-temperature nuclear process heat. In order to achieve competitive efficiencies, both processes require high-temperature operation (~850°C). Thus these hydrogen-production technologies are tied to the development of advanced high-temperature nuclear reactors. High-temperature electrolytic water-splitting supported by nuclear process heat and electricity has the potential to produce hydrogen with overall thermal-to-hydrogen efficiencies of 50% or higher, based on high heating value. This efficiency is near that of the thermochemical processes [5, 6], but without the severe corrosive conditions of the thermochemical processes and without the fossil fuel consumption and greenhouse gas emissions associated with hydrocarbon processes.

A research program is under way at the Idaho National Laboratory (INL) to simultaneously address the technical and scale-up issues associated with the implementation of solid-oxide electrolysis cell technology for efficient hydrogen production from steam. We are coordinating a progression of electrolysis cell and stack testing activities, at increasing scales, along with a continuation of supporting research activities in the areas of materials development, single-cell testing, detailed computational fluid dynamics (CFD) analysis and system modeling.

The experimental program at INL includes a range of test activities designed to characterize the performance of solid-oxide cells operating in the electrolysis mode. Small-scale activities are intended to examine candidate electrolyte, electrode, and interconnect materials with single cells and small

stacks. Initial cell and stack performance and long-term degradation characteristics have been examined. Larger scale experiments are designed to demonstrate the technology and to address system-level issues such as hydrogen recycle and heat recuperation.

The focus of this paper is the performance assessment of single electrode-supported cells operating in the electrolysis mode. In the fuel-cell mode of operation, anode-supported cells represent the state of the art in terms of performance [7]. Since the electrolyte generally represents the highest resistivity layer in the cell, decreasing its thickness can lead to improved performance. The nickel cermet material (anode in the fuel cell mode, cathode in the electrolysis mode) has relatively high electronic conductivity and is therefore a logical choice for use as the mechanical support layer in electrode-supported cells. In an anode-supported SOFC, the anode is typically 1 – 1.5 mm in thickness while the electrolyte thickness can be as low as 10 μm. In the electrolysis mode, it may be preferable to use an oxygen-electrode-supported cell [8], to reduce the concentration overpotential associated with steam diffusion through the thickness of the electrode toward the functional layer. In the fuel-cell mode, the steam diffusion away from the functional layer can be more readily pressure-driven. The oxygen-side electrode material for the present cells is lanthanum-strontium manganite (LSM). This layer is screen-printed on the cells, with a thickness of about 90 μm. The cells were fabricated by St. Gobain High-Performance Materials, and supplied to the Idaho National Laboratory via a CRADA agreement.

This paper provides a detailed overview of the apparatus that was developed for testing single electrode-supported cells in the electrolysis mode. Preliminary test results are also provided.

NOMENCLATURE

F	Faraday number, 96487 C/mol
ASR	area-specific resistance, Ohm·cm^2
ΔG_f	gibbs energy of formation, J/mol
i	current density, A/cm^2
I	current, A
$\dot{N}_{H_2}$	molar hydrogen production rate, mol/s
N_{O2prod}	number of oxygen equivalents
p	pressure, kPa
p_{std}	standard pressure, kPa
q''	heat flux, W/cm^2
Q_M	molar flow rate, mol/s
Q	volumetric flow rate, sccm
R_u	universal gas constant, J/mol·K
T	temperature, K
T_{dp}	dewpoint temperature
U_{H2O}	steam utilization, %
V_N	Nernst potential, V
V_{cell}	cell operating voltage, V
V_{OC}	open-cell voltage, V
V_{tn}	thermal neutral voltage, V
y	mole fraction
ρ_M	standard-state molar density, mol/m^3

SINGLE-CELL TEST APPARATUS

The test fixture and test stand designed for performance evaluation of electrode-supported single cells will now be described. This version of the test fixture is designed to evaluate the performance of individual cells without the complicating effects of interconnects. A modified version of this test fixture could be used to test individual cells plus interconnects.

Referring to the exploded view provided in Fig. 1, a steam hydrogen mixture enters through a ¼-in inconel coiled tube into the inlet hole in the bottom of the Hastelloy-X (HastX) base plate. It then flows through a diverging flow channel milled into the HastX base plate and passes through a slot in the bottom of the alumina cell holder. The slots can be seen in Fig 2. An alumina felt gasket is used to seal the HastX base plate against the alumina cell holder. The flow then passes under the cell through a corrugated/perforated nickel flow field. The flow field establishes the gap for the steam/hydrogen flow channel under the cell while also serving as an electrical conductor. A 0.254 mm (0.010 in) nickel foil underneath the

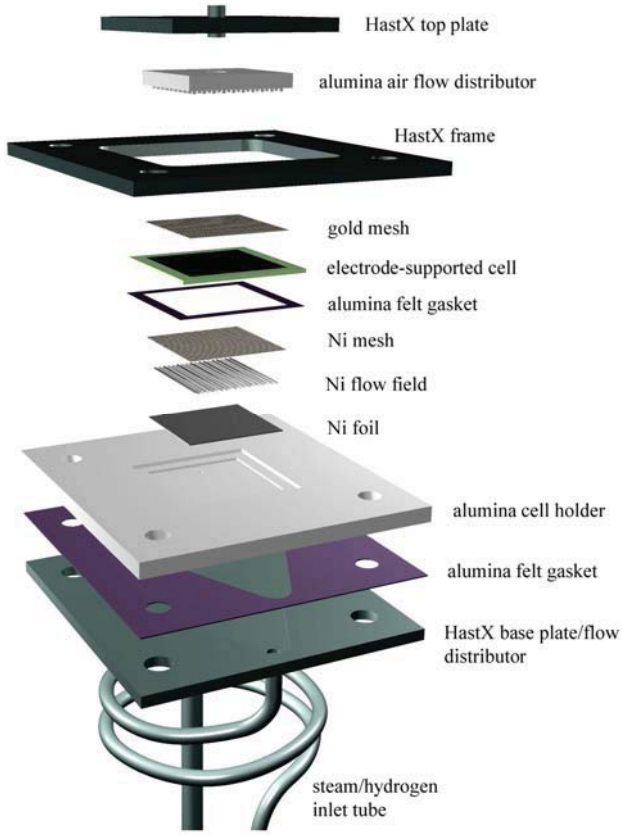

Figure 1. Exploded view of cell fixture.

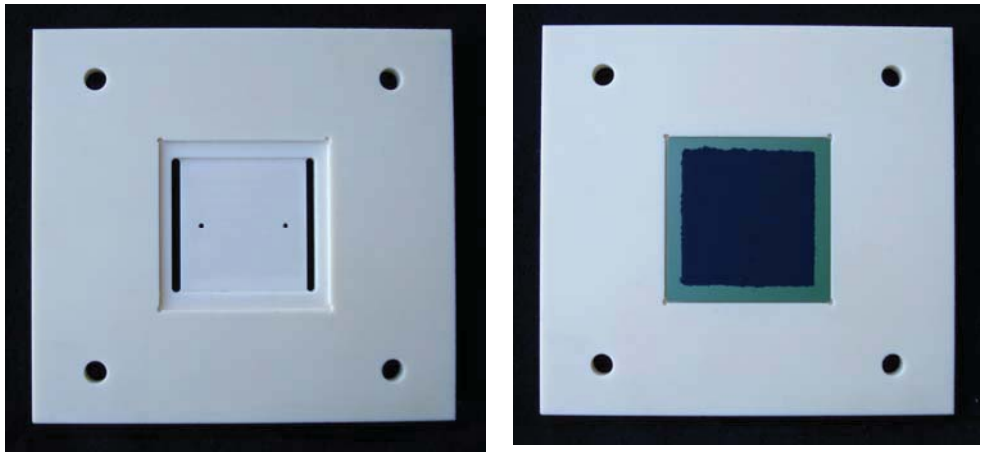

(a) (b)

Figure 2. (a) alumina cell holder; (b) cell holder with cell in place.

flow field serves as a current collector. The Ni foil, flow field, and mesh are sized to fit into the inner square recess machined into the alumina cell holder. Alumina was selected as the cell holder and air flow distributor material in order to minimize the potential for chromium poisoning of the cell electrodes. The cell holder was machined in the bisque state and then fired. During firing the bisque alumina shrinks by about 15%. This shrinkage must be taken into account when doing the machining such that the desired dimensions are achieved in the final dense alumina part.

A gold wire in direct contact with the nickel foil serves as the steam/hydrogen-side power lead and voltage tap. The wire just fits in one of the grooves of the flow field. The two ends of this wire are fed out through the two small holes shown in the bottom of the alumina cell holder, visible in Fig. 2(a).

After passing along the bottom of the cell, the steam/hydrogen flow exits the alumina cell holder through a second slot, flows through a converging passage in the HastX base plate, and out through an 3/8-in OD inconel outlet tube. The outlet tube is sized larger than the inlet tube in order to minimize back pressure on the cell seals to prevent leakage.

The cell is placed on a shelf milled into the alumina cell holder just above and in contact with the Ni mesh (see Fig. 2 (b)). The cell dimensions are 5 cm x 5 cm, 1.5 mm thick. A nickel paste was used to enhance electrical contact between the cell and the nickel mesh, flow field, and foil. An alumina felt gasket is placed on the shelf underneath the cell to help with sealing. In addition, for sealing, an alumina-based ceramic paste (Aremco Products, Ceramabond 552) is distributed around the top outer edge of the cell to seal the gap between the cell and the alumina cell holder.

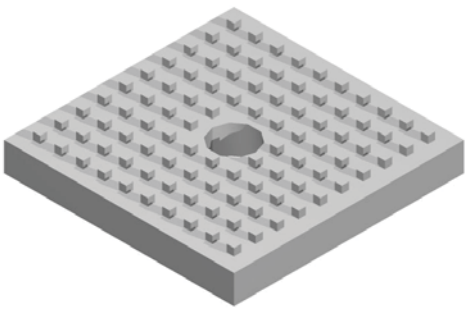

Figure 3. Alumina air flow distributor.

On the air side of the cell, a gold mesh contacts the air-side electrode. This gold mesh is held against the air-side electrode by the alumina air flow distributor. The air flow distributor has an array of square protuberances milled into its surface (see Fig. 3), creating a gap for air flow while also compressing the gold mesh against the air-side electrode. A gold wire is positioned in one of the grooves, in contact with the gold mesh, for current collection. One end of this wire is used as a power lead and the other end is used as a voltage tap.

Air is introduced to the top side of the cell through an inlet tube welded to the HastX top plate. This tube protrudes slightly into a central hole in the alumina air flow distributor. A seal was formed between the HastX top plate and the alumina air flow distributor by means of an alumina felt gasket. After exiting the central hole in the air flow distributor, the air impinges on the cathode side of the cell and flows radially outward through the array of protuberances. The air then exits into the furnace volume.

A fixed compressive load is applied to the entire cell stackup between the alumina cell holder and the HastX top plate by means of weights, as shown in the test stand overview, Fig. 4. This load simultaneously compresses the cell against the nickel mesh, flow field and foil on the bottom steam/hydrogen side of the cell and against the gold mesh on the air side. It also compresses the cell against the seal around the outer edge of the cell which rests on the shelf milled into the alumina cell holder. The HastX weight plates are held in alignment by the upper portion of the threaded rods which extend upward for this purpose.

A fixed compressive load is independently applied between the HastX frame, the alumina cell holder, and the HastX base plate. This load is generated by the compression of four springs located under the test stand base support outside of the furnace. The springs will be compressed a fixed amount

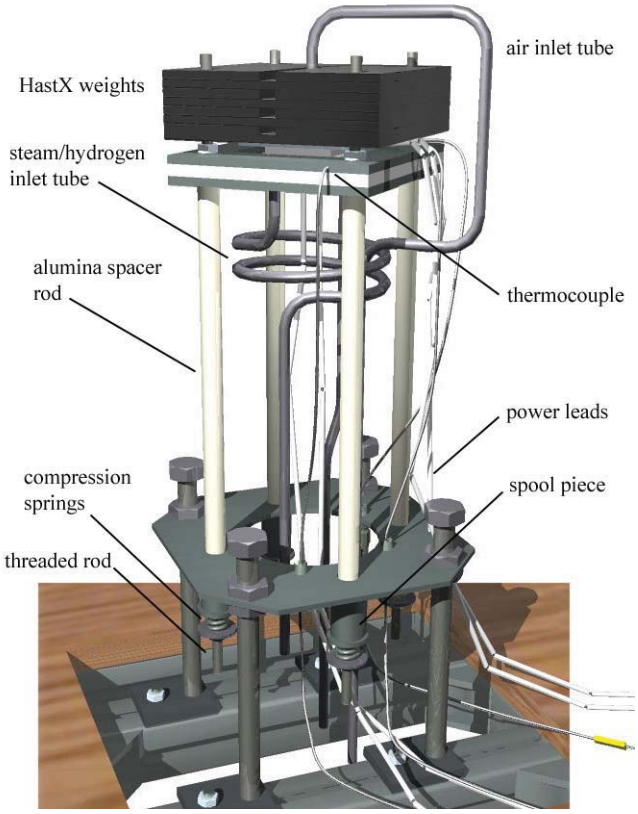

Figure 4. Test stand overview.

that is determined by the height of the spool pieces by tightening a nut on the threaded rods. The threaded rods are fed through the alumina spacer tubes. These spacer tubes determine the height of the cell holder inside the furnace. The spring-generated load is intended to compress the seal between the cell holder and the base plate. This seal was formed by alumina felt impregnated with alumina slurry. A nut is visible on the threaded rods in Fig. 4 just above the HastX frame and below the weight plates. This nut represents the upper stop for this compressive load. The extension of the threaded rods above the nuts is for the purpose of aligning the weight plates. Note that the weight plates are floating above these nuts since they are resting on the HastX top plate.

A photograph of the test stand installed in the furnace base is provided in Fig. 5. Note that the base support is located outside of the furnace. Holes were drilled in the bottom of the kiln for pass-through of the flow tubes, the alumina spacer rods, power leads and instrumentation.

A process flow diagram for the experimental apparatus used for single-cell testing is presented in Fig. 6. Primary components include gas supply cylinders, mass-flow controllers, a heated water-bath humidifier, on-line dewpoint sensors, temperature and pressure measurement, high temperature furnace, and the solid oxide electrolysis cell. Nitrogen is used as an inert carrier gas. Inlet flow rates of nitrogen, hydrogen, and air are established by means of precision mass-flow controllers. Hydrogen is included in the inlet flow as a reducing gas in order to prevent oxidation of the Nickel cermet electrode material. Air flow to the cell is supplied by the shop air system, after passing through a two-stage extractor / dryer unit. The cathode-side inlet gas mixture, consisting of hydrogen and nitrogen is mixed with steam by means of a heated humidifier. The dewpoint temperature of the nitrogen / hydrogen / steam gas mixture exiting the humidifier is monitored continuously using a precision dewpoint sensor. All gas lines located downstream of the humidifier are heat-traced in order to prevent steam condensation.

CELL REDUCTION

The electrode-supported cells tested in this study are supported by the porous 1.5 mm thick steam/hydrogen electrode whose initial composition is nickel oxide and YSZ. The nickel oxide must be reduced to nickel metal in order for the electrode to become electronically conductive. This reduction process is accomplished by exposing the electrode to increasing levels of hydrogen gas at 900°C, as indicated in Table 1. The initial heatup of the cell (step 0) is performed under inert gas at a heatup rate of 1°C/min to 900°C. The cell is then exposed to varying nitrogen/hydrogen/steam gas mixtures for the time durations indicated in the table. The steam was introduced by bubbling the nitrogen/hydrogen gas mixture through a room-temperature water bath (humidifier). The corresponding steam flow rates can be calculated based on the nitrogen and hydrogen flow rates and the bath temperature. These calculated steam flow rate values are listed in the table. The steam/hydrogen electrode of the reduced cell is silver/gray in color.

Figure 5. Test stand installed in furnace base.

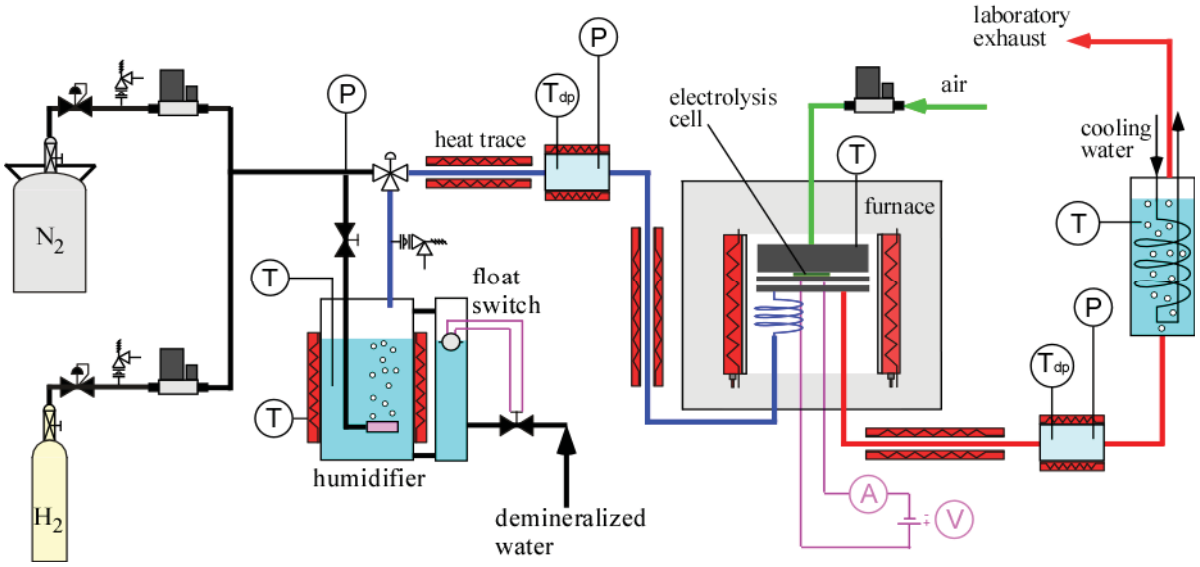

Figure 6. Process flow diagram for single-cell test apparatus.

TEST PROCEDURE

After the cell reduction procedure is completed, performance testing can be initiated. Test conditions can be determined as follows. Specify the cell active area and maximum desired current density. The nominal active area for the cells in this study is 16 cm^2. The maximum current density is usually set such that the maximum cell voltage is near the thermal neutral voltage (V_{tn} = 1.287 V at 800°C) [9]. Once the current density and cell area are known, the total cell current is known ($I = i \times A_{cell}$) and the molar hydrogen production rate can be determined directly from Faraday's law:

$$Q_{M,H_2,prod} = \frac{I}{2F} \tag{1}$$

This molar value can be converted to a standard volumetric flow rate (e.g., sccm) by dividing by the standard-state molar density, ρ_M = 44.615 mol/m^3.

A desired value for maximum steam utilization can then be specified. Depending on the objective of the test, this value could range from 0.2 – 0.9. Low values of steam utilization generally yield better cell performance in the electrolysis mode. High values can cause localized steam starvation and corresponding reduced cell performance. Analysis of large-scale systems has indicated that overall system performance drops off for steam utilization values below ~0.5, but is fairly flat above that value [10]. Once the desired steam utilization is specified, the required inlet steam flow rate can be determined from

$$Q_{H_2O,i} = \frac{Q_{H_2,prod}}{U_{H_2O}} \tag{2}$$

Since steam is introduced in this case using a humidifier, the steam flow rate depends on both the inlet dewpoint temperature, which is approximately the same as the humidifier bath temperature, and the flow rates of nitrogen and hydrogen. So the inlet dewpoint temperature must be specified. Nitrogen is included as an inert carrier gas to enable higher total steam flow rates and to allow for independent variation of the steam and hydrogen compositions in the inlet flow.

For testing in the electrolysis mode, a reasonably high inlet dewpoint temperature is required, typically 60 – 70°C. Once the inlet dewpoint temperature is specified, the corresponding inlet mole fraction of steam is given by

$$y_{H_2O,i} = \frac{p_{sat}(T_{dpi})}{p_T} \tag{3}$$

where $P_{sat}(T_{dpi})$ is the vapor pressure of steam at the specified inlet dewpoint temperature, obtained from an appropriate correlation such as the Antoine equation. The total required inlet gas flow of nitrogen plus hydrogen can then be obtained from

$$Q_{gas,\,i} = Q_{H_2O,i}\frac{1 - y_{H_2O,i}}{y_{H_2O,i}} \tag{4}$$

The inlet flow rate of hydrogen can be determined by specifying the desired inlet mole fraction of hydrogen, typically 0.1 – 0.2. Inlet hydrogen is required to maintain reducing conditions on the nickel cermet material. The respective flow rates of hydrogen and nitrogen are then obtained from:

$$Q_{H_2,i} = \frac{y_{H_2,i}}{y_{H_2O,i}} Q_{H_2O,i} \tag{5}$$

$$Q_{N_2} = Q_{gas,i} - Q_{H_2,i} \quad (6)$$

Air is typically used on the oxygen side of the cell as a sweep gas in order to prevent buildup of pure oxygen. The flow rate of air is scaled with respect to the oxygen production rate,

$$Q_{O_2,prod} = Q_{H_2,prod} / 2 \quad (7)$$

as follows:

$$Q_{air} = \frac{N_{O_2 prod} Q_{O_2,prod}}{y_{O_2,air}} \quad (8)$$

where N_{O2prod} is a factor indicating the number of oxygen production equivalents desired in the sweep air and y_{O2}, air is the mole fraction of oxygen in the sweep gas ($y_{O2,\ air}$ = 0.21). We typically use N_{O2prod} = 1, which yields an outlet sweep gas mole fraction of oxygen equal to 0.347.

Once the cell operating temperature is selected (typically 800°C), the test conditions are fully specified.

PRELIMINARY TEST RESULTS

The first indication of cell performance that can be observed is the open-cell potential, which can be calculated using the Nernst equation:

$$V_N = \frac{-\Delta G_{f,H_2O}}{2F} - \frac{R_u T}{2F} \ln\left(\frac{y_{H_2O}}{y_{H_2} y_{O_2}^{1/2}}\right) + \frac{R_u T}{4F} \ln\left(\frac{p}{p_{std}}\right) \quad (9)$$

Generally, for single-cell testing, if the observed open-cell potential is different from the theoretical value by more than a few millivolts, there may be a problem with the cell such as gas leakage, a cracked cell, or a short circuit. Open-cell potentials observed for the cells tested in this study were all within 2 mV of the theoretical value given by Eqn. (9).

Initial electrolysis performance of these cells was evaluated by acquiring voltage-current polarization curves at three different operating temperatures. These polarization curves are presented in Fig. 7 as cell voltage versus current density. The inlet gas flow rates and dewpoint temperature used during these sweeps are indicated in the figure. The sweeps were performed by varying the applied cell operating voltage from a value just below the open-cell voltage to a value of 1.3 V, which is just above the thermal neutral voltage.

Area-specific resistance (*ASR*) values for the cells are plotted in Fig. 8 as a function of current density. These are "apparent" ASR values, defined by:

$$ASR = \frac{V_{cell} - V_{OC}}{i} \quad (10)$$

Initial performance of the St. Gobain cells was characterized by performing several DC potential sweeps. Results of these sweeps are presented in Figs. 7 and 8. The initial sweeps were performed at 800, 850, and 900°C with humidifier bath temperatures of 60 and 70°C. Sweeps performed with an inlet dewpoint temperature of 60°C are presented in Fig. 7 and those with an inlet dewpoint of 70°C are in Fig. 8. Each figure shows both a series the *V-i* polarization curves and a series of *ASR-i* curves. Negative values of current density on Fig. 7 correspond to the fuel cell mode of operation and positive values represent the electrolysis mode. The polarization curves are linear through the zero-current transition from fuel-cell mode to electrolysis mode, indicating that activation does not contribute significantly to the observed overpotentials. At higher current densities, the voltage-current density curves are nonlinear, curving upward at high values of current density, revealing the effects of steam starvation and mass transfer through the thick (1.5 mm) steam-side electrode. This effect is more noticeable in the lower dewpoint data of Fig. 7 than in Fig. 8.

Cell area-specific resistance values decrease with increasing operating temperature and increasing steam content. Initial low-current *ASR* values for the 60°C inlet dewpoint sweeps were 0.62, 0.52, and 0.48 Ohm·cm^2 at 800, 850, and 900°C, respectively. Corresponding values for the 70°C inlet dewpoint sweeps were 0.57, 0.48, and 0.41 Ohm·cm^2. These initial ASR values are quite good, as low as have been observed with the highest performing electrolyte-supported button cells tested at INL.

Hydrogen production rates during cell operation can be calculated based on cell current using Faraday's law. In addition, hydrogen production rates can be determined independently based on inlet and outlet dewpoint

Table 1. Cell electrode reduction procedure.

step	Hold time (min)	H_2 Flow rate (sccm)	T_{dp} (°C)	H_2O flow rate (sccm)	N_2 flow rate (sccm)	Air flow rate (sccm)	T_{cell} (°C)	y_{H2O}
0 (heatup)	n/a	0	bypass	0	500	500	1°C/min	0
1	75	80	bypass	0	500	580	900	0
2	7.5	160	bypass	0	500	660	900	0
3	7.5	160	22	20.8	500	660	900	0.031
4	5	320	22	25.9	500	820	900	0.031
5	5	500	22	23.7	250	750	900	0.031
6	5	500	22	15.8	0	500	900	0.031

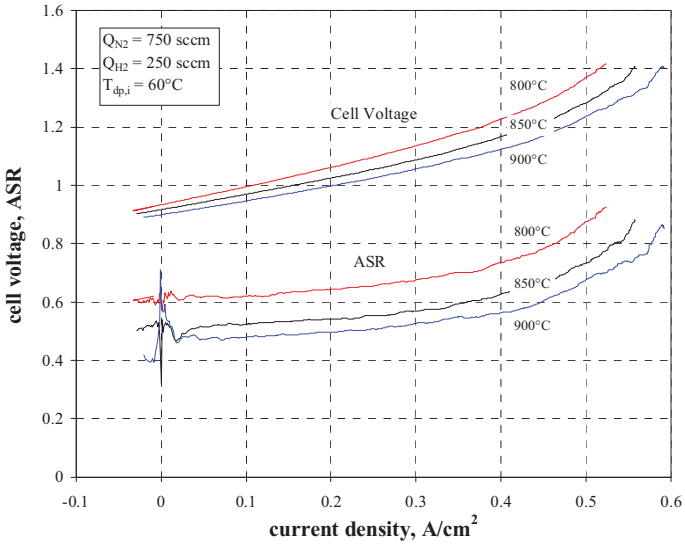

Figure 7. Cell voltage and ASR as a function of current density and operating temperature, initial sweeps, T_{dpi} = 60°C.

measurements. These measurements provide a direct indication of steam consumption rate, which on a molar basis is equal to the hydrogen production rate. Representative plots of inlet and outlet dewpoint temperatures and hydrogen production rates measured during a sweep are presented in Fig. 9. In this figure, the inlet dewpoint temperature is essentially constant, as expected, with a value of 67.2°C. The outlet dewpoint temperature decreases with increasing cell current, due to conversion of steam to hydrogen. Hydrogen production rates are also presented in the figure. The straight black line represents the hydrogen production rate based on cell current, using Faraday's law. The green line represents the hydrogen production rate base on the inlet and outlet dewpoint

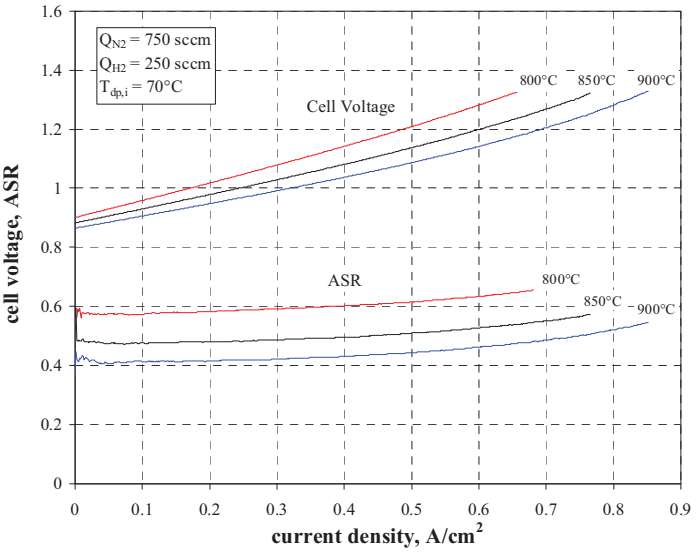

Figure 8. Cell voltage and ASR as a function of current density and operating temperature, initial sweeps, T_{dpi} = 70°C.

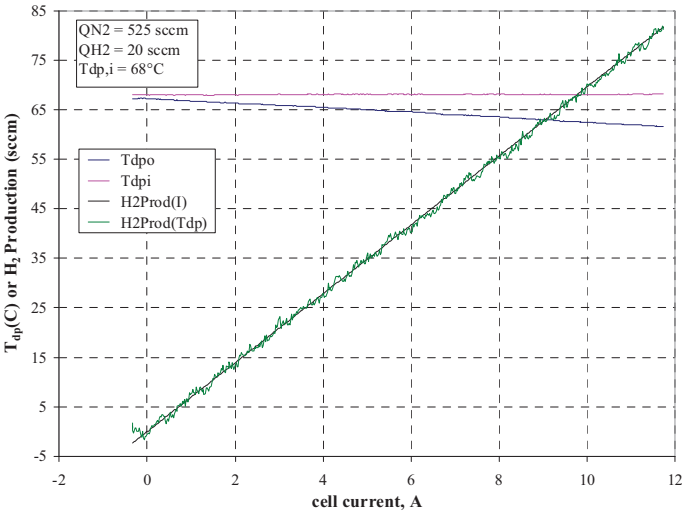

Figure 9. Dewpoint temperatures and hydrogen production rates as a function of cell current, T_f = 850°C, T_{dpi} = 68°C.

temperatures. This line naturally includes some scatter, but the agreement between the two independent measurements of hydrogen production rates is generally quite good, providing confidence in the experimental results.

Long-term operation of this cell was performed for over 600 hours at 850°C. During the first 250 hrs. of operation, the cell was operated at a voltage of 1.21 V, with a nominal inlet dewpoint value of 60°C. At this time, a series of sweeps was performed for comparison to the initial sweeps. These sweeps were performed at both 60 and 70°C inlet dewpoint temperatures. Subsequently, the long-term durability test was continued, retaining the higher inlet dewpoint value of 70°C. At an elapsed time of 590 hrs, a final sweep was performed.

Results of long-term durability testing for this cell are presented in Figs. 10 – 12. Fig. 10 shows the time history of cell voltage and current over 590 hours of elapsed test time.

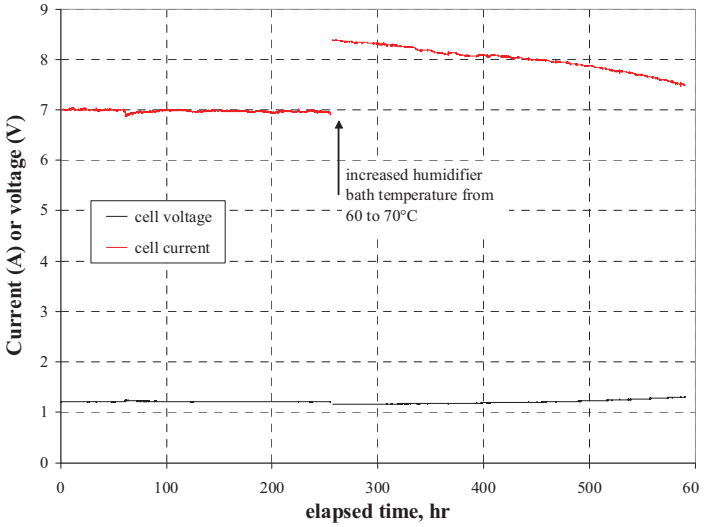

Figure 10. Cell voltage and current, long-term durability test.

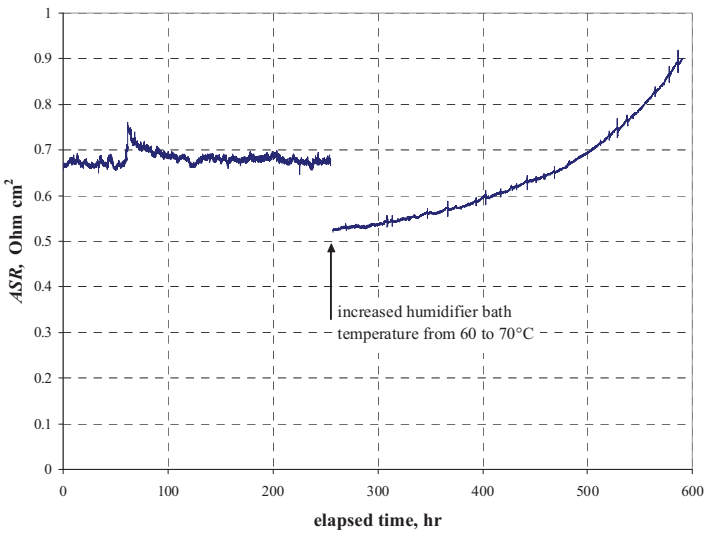

Figure 11. Cell area-specific resistance, long-term durability test.

There is a step change in voltage and current at ~260 hours, associated with an increase in the humidifier bath temperature from 60 to 70°C. This change in inlet steam content yielded a lower cell ASR value, resulting in a lower open-cell voltage, and a higher cell current at the same operating voltage. Cell voltage and current were very stable for the first 250 hrs of operation, indicating essentially zero performance degradation over that time period. However, after performing two sweeps at this time and increasing the bath temperature, performance degradation began to occur. This degradation is more evident in the plot of cell *ASR* presented in Fig. 11. For the first 250 hours of operation, the cell *ASR* at the fixed operating condition

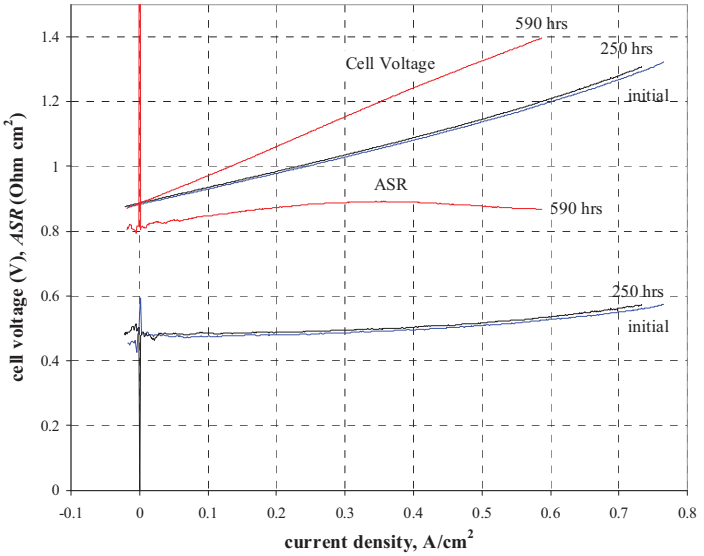

Figure 12. Cell voltage and ASR as a function of current density and cell operation time, T_{dpi} = 70°C.

of V_{cell} = 1.21 V was nearly constant at ~0.67 Ohm cm^2. After increasing the bath temperature, the *ASR* value immediately decreased to ~0.52 Ohm cm^2, as discussed previously in conjunction with the sweeps. Thereafter, the ASR value begins to increase, attaining a value of 0.90 Ohm cm^2 at 590 hrs. More durability testing with this type of cell will be required to determine the exact cause of the accelerated degradation that was observed with this cell after 250 hours. The most obvious culprit is the increased steam content, but the cell current also increased significantly and two sweeps were performed at 250 hours.

A final sweep was performed at 590 hrs. Fig. 12 presents cell voltage and *ASR* values as a function of current density for three sweeps with the humidifier bath at 70°C. Cell voltage and ASR values for the initial sweep and the 250-hr sweep are nearly identical. However, for the 590-hr sweep, cell voltage increases much more rapidly with current density. In addition, the ASR values are much higher at 590 hrs. The plot of *ASR* versus current density at 590 hrs has a different shape than for the earlier times. This difference in shape is at least partially due to the fact that the cell voltage for this sweep exceeded the thermal neutral voltage of 1.29 V. Beyond the thermal neutral voltage, the cell begins to heat up, which results in a lower *ASR* value.

SUMMARY AND CONCLUSIONS

An experimental apparatus has been successfully developed and demonstrated for testing single electrode-supported cells operating in the electrolysis mode. The cell holder is fabricated from alumina in order to minimize the potential for chromium poisoning of the cell electrodes. Electrical contact with the electrodes is accomplished using a gold mesh on the air-side and a nickel mesh on the steam/hydrogen side. The steam/hydrogen flow field is a corrugated/perforated nickel foil. Sealing of the cell in the alumina cell holder is accomplished using an alumina felt gasket and a ceramic paste. A fixed compressive load is applied to the entire cell stackup between the alumina cell holder and the top plate by means of weights. Reduction of the steam/hydrogen nickel cermet electrode is accomplished by exposing the electrode to increasing levels of hydrogen gas at 900°C. A detailed methodology for determining gas flow rates for cell testing has been provided. Initial electrolysis performance of these cells was evaluated by acquiring voltage-current polarization curves at three different operating temperatures over a voltage range from a value just below the open-cell voltage to a value of 1.3 V. Low-current-density ASR values were approximately 0.65, 0.50, and 0.42 Ohm·cm^2 at 800, 850, and 900°C, respectively. The apparent ASR values increase significantly with current density, reflecting the effect of steam consumption

ACKNOWLEDGMENTS

This work was supported by the Idaho National Laboratory, Laboratory Directed Research and Development

program and by the U.S. Department of Energy, Office of Nuclear Energy, Nuclear Hydrogen Initiative Program.

COPYRIGHT STATEMENT

REFERENCES

1. Lewis, D., "Hydrogen and its relationship with nuclear energy," *Progress in Nuclear Energy*, Vol. 50, pp, 394-401, 2008.
2. Forsberg, C. W., "Nuclear Hydrogen Production for Liquid Hydrocarbon Transport Fuels," Proceedings, AIChE Annual Mtg., pp. 7988-7995, 2005.
3. Hori, M., "Nuclear Energy for Transportation: Paths through Electricity, Hydrogen, and Liquid Fuels," *Progress in Nuclear Energy*, Vol. 50, pp. 411-416, 2008.
4. Scott, D. S., Smelling Land, the Hydrogen Defense against Climate Catastrophe, Canadian Hydrogen Association, 2007.
5. Yildiz, B., and Kazimi, M. S., "Efficiency of Hydrogen Production Systems Using Alternative Nuclear Energy Technologies," *Int. J. of Hydrogen Energy*, Vol. 31, pp. 77-92, 2006.
6. O'Brien, J. E., McKellar, M. G., and Herring, J. S., "Performance Predictions for Commercial-Scale High-Temperature Electrolysis Plants Coupled to Three Advanced Reactor Types," 2008 International Congress on Advances in Nuclear Power Plants, Anaheim, CA, June 8-12, 2008.
7. Blum, L., Meulenberg, W. A., Nabielek, and Steinberger-Wilkens, R., "Worldwide SOFC Technology Overview and Benchmark," *Int. J. Applied Ceramic Technology*, Vol. 2 No. 6, pp. 482-492, 2005.
8. Ni, M., Leung, M. K. H., and Leung, D. Y. C., „A Modeling Study on Concentration Overpotentials of a Reversible Solid Oxide Fuel Cell," *J. Power Sources*, Vol. 163, pp. 460-466, 2006.
9. O'Brien, J. E., "Thermodynamic Considerations for Thermal Water Splitting Processes and High-Temperature Electrolysis," 2008 ASME International Congress and Exposition, paper# IMECE2008-68880, Boston, Nov., 2008.
10. O'Brien, J. E., McKellar, M. G., Harvego, E. A., and Stoots, C. M., "High-Temperature Electrolysis for Large-Scale Hydrogen and Syngas Production from Nuclear Energy – System Simulation and Economics," International Conference on Hydrogen Production, ICH2P-09, Oshawa, Canada, May 3-6, 2009.